ChemComm

Improving LSPR Sensing Performance by Multilayered Composition Graded Ag-Cu Nanotriangle Arrays

Journal:	*ChemComm*
Manuscript ID	CC-COM-11-2018-008813.R1
Article Type:	Communication

Chemical Communications

COMMUNICATION

Improving LSPR Sensing Performance by Multilayered Composition Graded Ag-Cu Nanotriangle Arrays

Steven Larson,*[a] Zilan Yang[b] and Yiping Zhao[a]

Received 00th January 20xx,
Accepted 00th January 20xx

DOI: 10.1039/x0xx00000x

www.rsc.org/

Patterned nanotriangle arrays with composition graded and multilayered Ag-Cu were fabricated by a co-deposition and nanosphere lithography process. With the increase of number of the layers or constructing a continuum graded layer, the index sensitivity of resulting nanotriangles kept on increasing, indicating that graded boundaries can improve plasmonic resonance sensing.

Localized surface plasmon resonance (LSPR) based sensors have attracted great attention and have been widely studied over the past decades.[1-4] These sensors are compact, durable, repeatable, and more reliable than traditional sensors, offering real-time and label-free chemical and biological detection.[2, 5] They are characterized by two important parameters, their resonance wavelength shift with respect to changes in the local index of refraction, refractive index sensitivity (RIS) and figure of merit (FOM) which is the RIS divided by the full width at half-maximum (FWHM) of the spectral resonance peak, λ_0.[6] Most studies focus on improving the RIS and FOM through changes in the morphology of the sensor including structures as thin films[7], nanorods[8], nanospheres[9], nanopyramids[10], nanohelix[11], nanobranches[12], nanostars[13], nanotriangles (NTs)[14], and many others.[15] These traditional approaches generally have RIS from 50 to 250 nm/RIU with FOM in the single digits.[2, 16] However, more recent studies have shown that tuning the permittivity by changes in material and composition could significantly increase RIS without changing the structure. [11, 17-21] Taking a spherical nanoparticle as an example its LSPR wavelength can be approximated by $\mathrm{Re}(\varepsilon_m) = -2\varepsilon_d$ where $\mathrm{Re}(\varepsilon_m)$ is the real part of the dielectric function of the sensing material and ε_d is the dielectric function of the local environment.[6] Therefore, the RIS is determined by the dispersion of $\mathrm{Re}(\varepsilon_m)$ versus the wavelength. If $\left.\frac{dRe(\varepsilon_m)}{d\lambda}\right|_{\lambda=\lambda_0}$ is small, the same change of ε_d would induce a larger change in λ_0.[22] Thus, if one can tune the slope of the dispersion of $\mathrm{Re}(\varepsilon_m)$ of the plasmonic material, one can increase the RIS. Based on previous work done by us and others, using metal-metal or metal-dielectric composite nanostructures, one could systematically improve the RIS for LSPR sensors. [11, 17] In this communication, we will demonstrate an alternative strategy to systematically tune the RIS of plasmonic nanostructures, the use of composition graded Ag-Cu multilayer or continuum composition graded Ag-Cu layer.

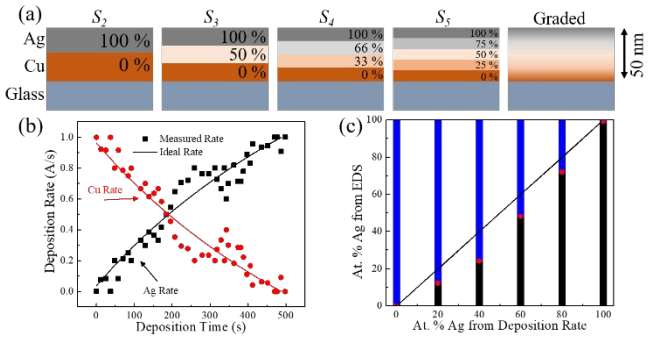

Figure 1: (a) Diagram of the layered structure; (b) the total thickness dependent Cu and Ag deposition rates for continuum graded nanotriangle fabrication; (c) the plot of atomic percentage of Ag in composite thin films determined by EDS versus the composition calculated from Ag and Cu deposition rates. The solid black line represents $y = x$.

The graded and multilayered Ag-Cu nanotriangle structures were fabricated through a combination of multistep dual electron beam deposition and nanosphere lithography.[15, 18, 23] The substrates used were polystyrene nanosphere (diameter D = 500 nm) monolayers on glass slides prepared by a water-air interface method.[24] **Figure 1a** illustrates the general layered structures and corresponding compositions of the deposited films. For the sake of comparison, we keep the average Ag and Cu composition at a constant 1:1 ratio, and the total thickness of the multilayer to 50 nm (quartz crystal microbalance reading). As the number (i) of layers increases, the corresponding layer thickness decreases to 50 nm/i, while the Ag composition of Ag-Cu composite layer varies from 0 at.% to 100 at.% with an increment of 100 at.%/(i – 2). Each sample is detonated as S_i. The single layered sample (S_1) was a 50 at.%

[a] Department of Physics and Astronomy, University of Georgia, Athens, GA, 30602
[b] College of Engineering, University of Georgia, Athens, GA, 30602
Electronic Supplementary Information (ESI) available: experimental details including fabrication and characterization, AFM images, XRD patters and crystal size estimates, ellipsometry measurements and figure of merit calculations. See DOI: 10.1039/x0xx00000x

Ag and 50 at.% Cu composite film. For the two-layered sample (S_2), 25 nm of Cu was deposited first, then 25 nm of Ag. The three-layered sample (S_3) has 16.6 nm of Cu, 16.7 nm of a 50 at.% - 50 at.% Ag-Cu composite, and 16.7 nm of Ag capping layer, and so on. For the continuum composition graded thin film deposition, the deposition rates of Ag (R_{Ag}) and Cu (R_{Cu}) were continuously tuned as shown in **Figure 1b**: initially R_{Cu} was 1 nm/s while R_{Ag} was zero; during the growth process, R_{Cu} was continuously decreased (till zero) while R_{Ag} was constantly increasing till a maximum, 1 nm/s. The final total thickness of Cu and Ag was 24 nm and 26 nm, respectively, with a Cu composition ~ 50 at.%. To confirm the accuracy of the composition of the individual layers, Ag-Cu composite thin film samples were deposited with constant R_{Ag} : R_{Cu} ratio and their composition was investigated by the energy-dispersive X-ray spectroscopy as shown in **Figure 1c**. Overall the Ag composition was slightly lower than expected. This inconsistency could be attributed to the lower sticking coefficient of Ag as compared to Cu which is partly due to their difference in melting points (T_{Ag} = 960 °C and T_{Cu} = 1091 °C). [25, 26] This effect has been well studied in literature and is a common problem with Ag based depositions.[27, 28] During all depositions, the substrates were rotated azimuthally at a constant speed, 60 rpm.

In the supporting information **Figure S2** shows typical AFM topographic images of the deposited samples. All the structures were NTs in a standard hexagonal lattice predicted by nanosphere lithography. Overall the NTs are consistent in size and shape with an average height h_p = 230 ± 20 nm as defined in **Figure S2** and a measured thickness of 28 ± 3 nm. The structure of the NT was confirmed by SEM and a representative SEM image of the graded sample is shown in **Figure S3**. The reduction in NT thickness is consistent with nanosphere lithography and is due to a relatively low sticking coefficient for Ag and Cu, re-emission, and QCM calibration. Some residual polystyrene is visible which have been shown previously to not appreciably affect the optical properties of the NT arrays.[17] The apexes of the plane NTs were not sharp due to the fact that both Ag and Cu sources have a 10° vapor incident angle with respect to the substrate surface normal and the substrate was rotated continuously.[24] Any composition inhomogeneity across the NTs were compensated by such a substrate rotation.[18]

Figure 2a shows the optical extinction spectra of the multilayered and graded NT arrays. Overall, all the samples present a strong peak at the wavelength λ_0 ~ 1000 nm and a small peak at λ ~ 500 nm. **Figure 2b** plots both λ_0 and corresponding FWHM of the strong extinction peak as a function of the number of layers. Both λ_0 (= 1000 ± 25 nm) and

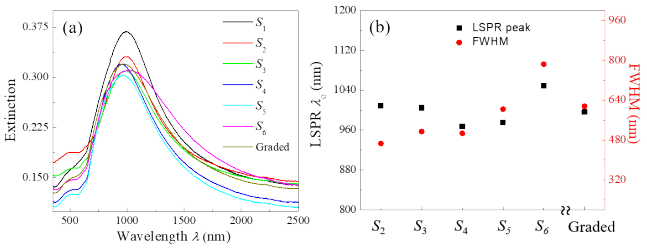

Figure 2: (a) Experimentally measured extinction spectra of different NT samples, and (b) the extracted LSPR peak location λ0 and corresponding FWHM values versus sample layers.

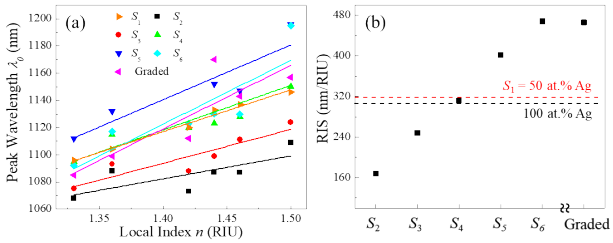

Figure 3: (a) The LSPR peak shift versus the refraction index *n* of the solutions different NT samples immersed in; and (b) the plot of RIS of different NT samples versus the sample layers. The black and red dashed lines indicate the RIS of pure Ag and 50 at.% AgCu NT samples.

the FWHM (= 500 ± 90 nm) do not change significantly. These peaks are consistent with other studies on Ag NTs.[17, 18] Our previous study of composite Ag-Cu NTs also demonstrated similar peaks when the composite was roughly 50 at.% Ag.[29]

The RIS characterization of each sample was conducted by immersing each sample in acetone, 1-hexanol, chloroform, carbon tetrachloride, and toluene, subsequently, in a quartz cuvette, and the corresponding extinction spectra were measured in each solvent. For all the samples, as the local index of refraction increased, λ_0 redshifted. **Figure 3a** plots the shift of λ_0 versus the local refractive index *n*. Each sample shows a linear dependence of λ_0 versus *n*. The slope of the linear fitting is the RIS. **Figure 3b** shows the RIS as a function of the number of layers. When the layer *i* changes from 2 to 6, the RIS increases almost linearly with *i*, from RIS = 168 nm/RIU to 468 nm/RIU. When the structure becomes the continuum graded layer, the RIS = 466 nm/RIU, which suggests that when $i \geq 6$, RIS reaches the maximum. Note that when *i* = 1, RIS = 320 nm/RIU, which has a similar RIS of Sample S4. For a pure Ag NTs with the same size, its RIS = 312 nm/RIU, which is also close to Sample S4 value. Clearly compared to pure Ag NTs or single layered composite Ag-Cu NTs, the multilayered composition graded Ag-Cu NTs shows opposite trend: when $i \leq 4$, the LSPR sensing performance is worse; when $i > 4$, the LSPR sensing performance is significantly improved. Such a fact provides a novel strategy to tune the plasmonic properties of a nanostructure: even with the fixed size, shape, thickness, and composition of a plasmonic structure, the composition graded multilayered structures can be used to systematically tune the plasmonic behavior. When the number of layers is few, due to strong scattering effect at the interface between adjacent layers, the plasmonic performance will be deteriorated; however, when *i* is large, or even approach to, and the graded layers could continuously attenuate the propagation wave number, which may minimize the loss, thus improve the plasmonic performance.

In fact, by investigating the real part of the effective dielectric function ε_1 of the resulting films, we notice that the slope $\left.\frac{d\varepsilon_1}{d\lambda}\right|_{\lambda\sim\lambda_0}$ does change with *i*. **Figure 4a** plots the effective ε_1 of the layered and graded thin films extracted from ellipsometry measurements. The overall shapes of ε_1 versus λ relationship are very similar for all the samples, but the slope $\left.\frac{d\varepsilon_1}{d\lambda}\right|_{\lambda\sim\lambda_0}$ for different sample is different. In general, the slope becomes

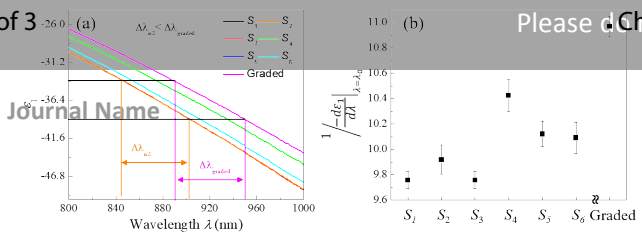

Figure 4: (a) The extracted real dielectric spectra ε_1 obtained from ellipsometry measurements of thin films for corresponding NT samples, and (b) the plot of numerically extracted $\left[\frac{d\varepsilon_1}{d\lambda}\Big|_{\lambda\sim\lambda_0}\right]^{-1}$ versus the sample layers at λ_0 ~ 965 nm

smaller when *i* increases. **Figure 4b** plots slope $\left[\frac{-d\varepsilon_1}{d\lambda}\Big|_{\lambda\sim\lambda_0}\right]^{-1}$ extracted numerically from **Figure 4a** versus *i* at λ_0 ~ 965 nm by linear fitting the data from 950 - 980 nm and extracting the slope. The trend in the change of $\left[\frac{d\varepsilon_1}{d\lambda}\Big|_{\lambda\sim\lambda_0}\right]^{-1}$ is consistent with the RIS shown in **Figure 3b**. This infers that we should see an increase in RIS if the structure follows the approximation of a spherical particles resonances as other NT arrays have demonstrated.[17, 29]

In a summary, here we demonstrate a novel strategy to systematically tune the plasmonic property of a nanostructure in addition to size, shape, thickness, and composition, i.e., to design nanostructures with composition graded multilayered or continuum composite films. It is expected that when the layer number is large enough, the plasmonic performance of the resulting nanostructures can improved significantly. We have experimentally demonstrated such a strategy by investigating the NT arrays made of the composition graded multilayer. When the layer number is larger than 4, the RIS of local index sensor is improved significantly. It is expected that when such a strategy is combined with other strategies, such as tuning the size, shape, gap or thickness, a better overall plasmonic optimization structure could be formulated. In addition, further understanding of how plasmonic waves propagate in these composition (or index) graded structures may shine some lights on designing better plasmonic waveguides or related applications.

Conflicts of interest

There are no conflicts to declare.

Notes and references

1 M. R. Jones, K. D. Osberg, R. J. Macfarlane, M. R. Langille and C. A. Mirkin, Chemical Reviews, 2011, 111, 3736-3827.
2 K. M. Mayer and J. H. Hafner, Chemical Reviews, 2011, 111, 3828-3857.
3 M. E. Stewart, C. R. Anderton, L. B. Thompson, J. Maria, S. K. Gray, J. A. Rogers and R. G. Nuzzo, Chemical Reviews, 2008, 108, 494-521.
4 M. Li, S. K. Cushing and N. Wu, Analyst, 2015, 140, 386-406.
5 I. E. Sendroiu, M. E. Warner and R. M. Corn, Langmuir, 2009, 25, 11282-11284.
6 Y. Li, Plasmonic optics: theory and applications, SPIE Press, 2017.
7 M. Svedendahl, S. Chen, A. Dmitriev and M. Kall, Nano Letters, 2009, 9, 4428-4433.
8 C.-D. Chen, S.-F. Cheng, L.-K. Chau and C. R. C. Wang, Biosensors and Bioelectronics, 2007, 22, 926-932.
9 Z.-Z. Gu, R. Horie, S. Kubo, Y. Yamada, A. Fujishima and O. Sato, Angewandte Chemie, 2002, 114, 1201-1204.
10 P.-Y. Chung, T.-H. Lin, G. Schultz, C. Batich and P. Jiang, Applied physics letters, 2010, 96, 261108.
11 H.-H. Jeong, A. G. Mark, M. Alarcón-Correa, I. Kim, P. Oswald, T.-C. Lee and P. Fischer, 2016, 7, 11331.
12 H. Chen, X. Kou, Z. Yang, W. Ni and J. Wang, Langmuir, 2008, 24, 5233-5237.
13 S. K. Dondapati, T. K. Sau, C. Hrelescu, T. A. Klar, F. D. Stefani and J. Feldmann, ACS Nano, 2010, 4, 6318-6322.
14 B. Sepulveda, P. C. Angelome, L. M. Lechuga and L. M. Liz-Marzan, Nano Today, 2009, 4, 244-251.
15 B. Ai and Y. Zhao, Nanophotonics, 2018, DOI: 10.1515/nanoph-2018-0105.
16 H. Liao, C. L. Nehl and J. H. Hafner, Nanomedicine, 2006, 1, 201-208.
17 S. Larson and Y. Zhao, The Journal of Physical Chemistry C, 2018, 122, 7374-7381.
18 W. Ingram, S. Larson, D. Carlson and Y. Zhao, Nanotechnology, 2016, 28, 015301.
19 G. Collins, E. K. McCarty and J. D. Holmes, CrystEngComm, 2015, 17, 6999-7005.
20 M. B. Cortie and A. M. McDonagh, Chemical Reviews, 2011, 111, 3713-3735.
21 S. Liu, G. Chen, P. N. Prasad and M. T. Swihart, Chemistry of Materials, 2011, 23, 4098-4101.
22 M. M. Miller and A. A. Lazarides, The Journal of Physical Chemistry B, 2005, 109, 21556-21565.
23 Y. He, J. Fan and Y. Zhao, Crystal Growth & Design, 2010, 10, 4954-4958.
24 I. Whitney, H. Yizhuo, S. Keenan, M. D. William, Y. Dexian and Z. Yiping, Nanotechnology, 2016, 27, 385301.
25 R. O. Simmons and R. W. Balluffi, Physical Review, 1960, 119, 600-605.
26 J. A. Cahill and A. D. Kirshenbaum, The Journal of Physical Chemistry, 1962, 66, 1080-1082.
27 D. Flötotto, Z. M. Wang, L. P. H. Jeurgens, E. Bischoff and E. J. Mittemeijer, Journal of Applied Physics, 2012, 112, 043503.
28 B. Dick, M. J. Brett and T. Smy, Journal of Vacuum Science & Technology B, 2003, 21, 2569-2575.
29 I. Whitney, L. Steven, C. Daniel and Z. Yiping, Nanotechnology, 2017, 28, 015301.